

Central pattern generators evolved for real-time adaptation to rhythmic stimuli

Alex Szorkovszky^{1,2,*}, Frank Veenstra² and Kyrre Glette^{1,2}

¹RITMO Centre for Interdisciplinary Studies in Rhythm, Time and Motion,
University of Oslo, Oslo, Norway

²Department of Informatics, University of Oslo, Oslo, Norway

* Email: alexansz@ifi.uio.no

Abstract

For a robot to be both autonomous and collaborative requires the ability to adapt its movement to a variety of external stimuli, whether these come from humans or other robots. Typically, legged robots have oscillation periods explicitly defined as a control parameter, limiting the adaptability of walking gaits. Here we demonstrate a virtual quadruped robot employing a bio-inspired central pattern generator (CPG) that can spontaneously synchronize its movement to a range of rhythmic stimuli. Multi-objective evolutionary algorithms were used to optimize the variation of movement speed and direction as a function of the brain stem drive and the center of mass control respectively. This was followed by optimization of an additional layer of neurons that filters fluctuating inputs. As a result, a range of CPGs were able to adjust their gait pattern and/or frequency to match the input period. We show how this can be used to facilitate coordinated movement despite differences in morphology, as well as to learn new movement patterns.

1 Introduction

Biologically inspired central pattern generators (CPGs) are useful for their properties, typical of self-organized systems, such as distributed control and robustness to perturbations [1, 2]. This allows adaptive behaviours such as compensation for physical damage [3] or walking in novel environments [4]. Spontaneous entrainment of motion patterns to sensory input is also expected from such systems, and adaptation of bio-inspired CPGs to body and environmental mechanics has indeed been widely demonstrated [5, 6, 7, 8]. Likewise, the movement pattern itself can be determined by interactions with the environment [9, 10].

While there typically exists a ‘natural’ gait frequency for a particular gait with a particular body (i.e. one that maximizes energy efficiency), it is often necessary to modulate one’s

gait frequency. A cat, for example, may need to walk at a slow pace in order to ambush its prey. For robots, being able to adapt to humans in their vicinity is an important goal, particularly for caring and collaborative applications [11]. For early humans, it is widely thought that the ability to synchronize movements with others was a crucial step in the evolution of social cognition [12, 13, 14]. This is therefore a relevant capability for socially responsive and intelligent robotics.

In vertebrates, gait pattern and frequency modulation are indirectly controlled by the intensity of the current from the brain stem, to which the spiking rates of locomotor neuron populations are sensitive [15]. Early bio-inspired robotics work attempted to replicate this emergent pattern generation, typically with continuous-time recurrent neural networks [16, 17]. This connectionist approach was largely abandoned in favour of more manageable coupled limit-cycle oscillators, where each parameter’s effect on the overall behaviour is predictable [1, 18, 19], particularly if the CPG outputs are mapped to workspace trajectories [20]. Hence, the problem of gait adaptation has become a matter of designing appropriate feedbacks or learning schemes for the designated control parameters. These continuous learning approaches have been highly successful for learning stable locomotion and adapting to unseen physical environments [21, 22].

Adapting to a social environment, however, is qualitatively different to adapting to a physical environment. One example of a social adaptation is imitation or learning by demonstration. This is now common in, for example, compliant robotic arms, where there are few constraints on movement [23]. However, for most CPG-based legged robot controllers, the range of available limit cycles is prescribed by design. Therefore, the potential for imitation and synchronization is relatively limited in most current legged robots.

The problem of large parameter spaces that comes with more flexible neuron models can be tackled using the same method by which nature succeeded to make animals roam the earth. Evolutionary methods are a useful tool for robotics, making use of the abundance of computing power now at our disposal [24, 25] and new algorithms for promoting diversity of designs [26, 27]. This has led to advances in morphology design [28], modular and soft robots [29, 30], and generative encodings [31].

While evolution and real-time adaptation may at first glance seem like unrelated processes working at very different time-scales, there are several ways in which evolution can facilitate adaptation. Evolution can, for example, globally optimize in the high-dimensional space of connection weights in recurrent neural networks so that a lower dimensional space of inputs encompasses a wide repertoire of output patterns [32, 33]. When applied to locomotion patterns, this dimensionality reduction can therefore simplify the task of online learning of which behaviours are most suitable in which state and environment, as is done in reinforcement learning [34], or the task of Hebbian learning of connection weights for higher-level control [35, 36]. Importantly, reactive controllers can also be optimized in advance for susceptibility to a wide range of inputs, allowing spontaneous compliant motion in an open-loop scenario.

Single-objective evolutionary algorithms were used in early work on connectionist CPGs, generally to optimize some combination of walking speed, regularity and stability measures

[17, 37]. These measures are often involved in trade-offs, meaning that despite the “hands-off” nature of evolutionary algorithms, fitness functions still needed to be carefully designed to weight each measure appropriately. The advent of multi-objective algorithms [26] allows these measures to be separated into their own fitness functions, so that a diverse range of controllers is generated along the Pareto front of non-dominated solutions [38, 39, 40]. Therefore, in addition to the advantages of evolutionary algorithms for highly flexible neural controllers, multi-objective evolution in particular also allows for correlational studies about their emergent properties, and for controllers to be hand-picked for different sets of capabilities after a single optimization process.

In this paper, we use multi-objective evolution to test the assumption that evolving CPGs for flexibility can facilitate rapid real-time gait adaptation. This contributes to bio-inspired robotics in two ways. Firstly, we demonstrate novel virtual robot quadrupeds that can entrain their locomotion to a range of rhythmic external inputs without physical coupling and without explicit feedback. This kind of automatic adaptation to social environments via audio and visual perception is common in humans, such as the tendency to synchronize when walking together [41]. While rhythmic entrainment to social partners has been demonstrated in virtual robots [42], this used relatively slow phase-based feedbacks in linear oscillators. Therefore, using neuromorphic CPGs can increase the naturalistic quality of multi-robot and human-robot interaction at the level of basic behaviours.

Secondly, we show how examining correlations between emergent properties of the CPGs can aid future design. Connectionist control systems are once again being increasingly employed in robotics, and these generally require searching through a large parameter space using automated processes such as reinforcement learning or genetic algorithms that target a desired ability [43, 44]. Identifying statistical trends between such abilities (costs or fitness functions) and features that can be more easily manipulated prior to optimization can greatly increase the efficiency of this time-consuming process [45].

For example, previous work with disembodied CPG architectures has suggested that both gait type and the sensitivity of oscillation period to neuron bias are important factors for entrainment ability [46]. We further test this correlation in an embodied context, where there is a simultaneous goal of upright walking. To test whether our results are dependent on the morphology of the embodied system, we use two quadrupeds that differ in limb length. Wide applicability is important for interaction between robots optimized for different environments, or those that adapt their morphology in real time [47].

First, using a multi-objective genetic algorithm and a fitness evaluation during which two control parameters are swept, we evolve populations of CPGs for flexible walking speed and direction. Then, for a subset of CPGs that emphasize different components of the objective function, we incrementally evolve robust filters for rhythmic (such as audio) input. We analyze the real-time entrainment performance of the robots as a function of the CPG properties, in particular the flexibility of the gait period and pattern. Finally, we discuss the implications of our results for understanding adaptive and imitative behaviour, as well as the potentials of our approach for multi-robot systems, human-robot interaction and autonomous learning.

2 Methods

2.1 Neuron model

The neural model is based on the Matsuoka neuron [48], a simple and popular model for robotics [8, 20, 49, 50, 51]. This is a biologically motivated yet abstract two-variable model:

$$t_0 \frac{du_i}{dt} = -u_i - av_i + I_i(t) \quad (1)$$

$$t_0 \frac{dv_i}{dt} = -\gamma v_i + bh(u_i) \quad (2)$$

where $h(u)$ is a rectified linear unit: $h(u) = 0$ for $u \leq 0$ and $h(u) = u$ for $u > 0$. Like many biological models, there is a fast “spiking” variable (u_i) and a slow “recovery” variable (v_i).

While this model produces patterns of spiking in a simple way, its linearity leads to a poor ability to adapt oscillation frequency [52]. Importantly, unlike biological neurons, the spiking rate is insensitive to changes in tonic input [53]. To address this shortcoming, we add a sigmoidal “deactivation” function to the fast variable u_i

$$t_0 \frac{du_i}{dt} = -u_i - aS(\kappa[u_i - u_0])v_i + c_i + d_i I_{DC} + I_{AC,i}(t) \quad (3)$$

$$t_0 \frac{dv_i}{dt} = -\gamma v_i + bh(u_i) , \quad (4)$$

where $S(x) = 1/(1 + \exp(x))$. In addition we introduce I_{DC} , a control parameter modelling the global brain stem input separately from fluctuating inputs $I_{AC,i}$ and a constant offset c_i . For a certain parameter range satisfying

$$c_i + d_i I_{DC} > u_0 + \frac{2}{\kappa} , \quad (5)$$

this reproduces the general nullcline shape, as well as the input-dependent firing rate, of biological neuron models [54]. The fast input is modelled:

$$I_{AC,i}(t) = G_i I_{in}(t) + I_{fb,i}(t) + \sum_{j \neq i} w_{ij} h(u_j(t) - \tau_{ij}) \quad (6)$$

where $I_{fb,i}$ is sensory feedback and I_{in} is the external input, G_i is input sensitivity, and w_{ij} is the synaptic weight and τ_{ij} the threshold for a connection from neuron j to neuron i .

2.2 CPG and Filter modules

The layout of the quadruped is shown in Figure 1A. This is a simplified version of the CPG layout in [15] containing one flexor-extensor pair per limb and several interneuron types. Our simplified model consists of three neurons per limb: one interneuron, a leg joint neuron (A) and a knee joint neuron (B). Each limb has identical parameters, and the connection weights are constrained to obey lateral symmetry. The ranges of the 23 neuron parameters

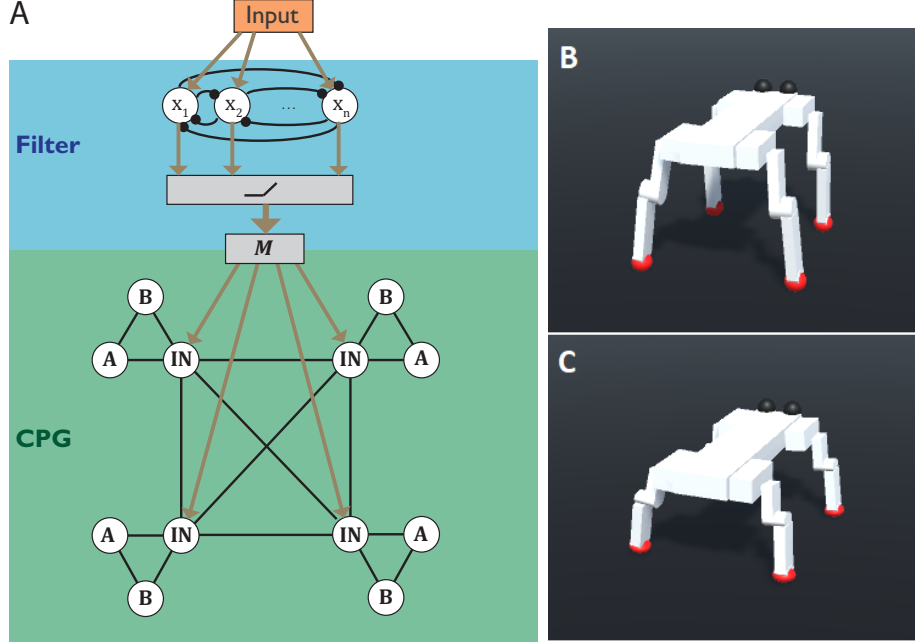


Figure 1: Panel (A) shows the layout of the robot controller. Circles denote modified Matsuoka neurons (n in the filter component, and 12 in the central pattern generator). Arrows denote one-way connections (either excitatory or inhibitory), lines ending in circles denote inhibitory connections, and regular lines denote mutual connections that may be excitatory or inhibitory. The modules are connected via n rectifying linear units with threshold τ_0 , followed by an n by 4 weight matrix \mathbf{M} . A/B: motor neurons; IN: interneurons. For this study, $n = 6$. (B): Open dynamic robot-based design. (C): Short-legged variant.

and connection weights are given in Supplementary Table S1. For the CPG module, $G_i = 0$ and $\tau_{ij} = 0$ within the CPG. Depending on the connection weights, which could be excitatory or inhibitory, and the brain stem drive, the CPG can autonomously generate coordinated oscillations in the motor neurons. Flexible movement was targeted for this autonomous behaviour in the first stage of evolution (see section 2.4).

A subset of the evolved CPGs with high fitness had filter modules evolved on top (see Section 2.5). The purpose of this layer is to preprocess and distribute descending rhythmic signals $I_{in}(t)$ for the CPG to entrain its oscillations to. This module had only inhibitory connections, no lateral symmetry, no feedback and no brain-stem control ($d_i = 0$). A non-zero threshold $\tau_{ij} = \tau_0$ was imposed between the filter outputs and CPG inputs so that the CPG received no input from the filter when $I_{in}(t) = 0$. The modules are unidirectionally linked by the weight matrix \mathbf{M} , with a wider range than the within-module weights w_{ij} (see Supplementary Table S2).

2.3 Robot simulation

The quadruped robots were simulated in the Unity game engine on a flat planar surface. The full-scale robot was based on the specifications of the Open Dynamic Robot [55]. The ‘short-legged’ version was identical, apart from a 40% reduction in upper leg length and a 33% reduction in lower leg length. The controllers were written in Python and interfaced with Unity using the Unity ML-agents package [56].

The CPG used a time interval of 8 ms while the physics simulation used a time interval of 20 ms, with decisions made every $\Delta t = 100$ ms. At each decision point, the CPG sent joint positions based on the changes in rectified motor neuron outputs since the previous simulation step $\Delta h(u_A(t))$ and $\Delta h(u_B(t))$:

$$\theta_{\text{leg}}(t) = \theta_{0,\text{leg}} + \theta_{\text{lim,leg}} \left[2S \left(\frac{2A}{\theta_{\text{lim,leg}}} \frac{\Delta h(u_A(t))}{\Delta t} \right) - 1 \right] + \theta_C \quad (7)$$

$$\theta_{\text{knee}}(t) = \theta_{0,\text{knee}} + \theta_{\text{lim,knee}} \left[2S \left(\frac{2B}{\theta_{\text{lim,knee}}} \frac{\Delta h(u_B(t))}{\Delta t} \right) - 1 \right] \quad (8)$$

where $S(x)$ is a logistic function, limiting the half-amplitude of motion of the upper leg and limb joints to $\theta_{\text{lim,leg}}$ and $\theta_{\text{lim,knee}}$, respectively, both of which are set to 90 degrees. The coefficients A and B , and the zero-angles are allowed to evolve, however with leg zero-angles $\theta_{0,\text{leg}}$ always positive and $\theta_{0,\text{knee}}$ always negative, corresponding to a full-elbow pose. The hip joint, perpendicular to the leg and knee joints, was kept at a constant but evolvable parameter $\theta_{0,\text{hip}}$. See Supplementary Table S3 for the ranges of these evolvable parameters. A control parameter θ_C was also added to the leg joint angle so that the forward position of the center of mass could be controlled in real time (see next section).

At each decision point, the CPG also received inputs processed from the body’s tilt, to use as stabilizing feedback inputs $I_{\text{fb},i}$. The sideways tilt (the sideways component of the unit vector normal to the top of the body) was input with opposite signs to the left and right limb motor neurons, with separate coefficients $q_{A,\text{side}}$ and $q_{B,\text{side}}$ for neurons A and B, respectively. Likewise, the front-back tilt (the upwards component of the unit vector normal to the front of the body) was input with opposite signs to the front and back limb inputs, with coefficients $q_{A,\text{front}}$ and $q_{B,\text{front}}$. These four coefficients were also evolved along with the CPG. The entire set of 32 parameters for the CPG and body was encoded as a sequence of integers, each taking a value between 1 and 10.

2.4 CPG evolution

We used the NSGA3 algorithm [26] in the DEAP Python package [57] to perform multi-objective optimization. This genetic algorithm preferentially selects non-dominated individuals (i.e. those on the Pareto front) for propagation to the next generation. Parameters used for the NSGA3 algorithm are given in Supplementary Table S4.

Unlike in [46] where each CPG was iteratively evaluated to explicitly select for change in period as a function of the brain stem drive I_{DC} , we instead swept I_{DC} during a single

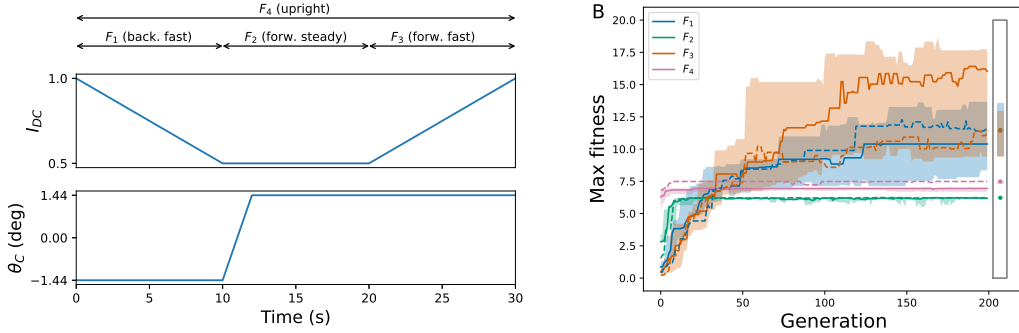


Figure 2: CPG evaluation and evolution. **(A)** Sweeping of control parameters I_{DC} and θ_C over the course of a single evaluation. The CPG undergoes a ‘burn-in’ period of 8s prior to the $t = 0$ mark. For the first two seconds of the simulation, the actuators are ramped from zero to the full CPG output. The arrows above show the measured fitnesses and targeted behaviours during each stage. **(B)** Maximum fitnesses vs generation. Solid lines: normal quadruped; dotted lines: short-legged variant. Each line is the median over 5 replicates. Shaded areas are the range over the 5 replicates for the normal quadruped. Areas inside the box on the right side of the plot are the final ranges of maximum fitness for the short-legged variant.

evaluation, and partially selected for variability in speed. This was to reduce the computational load of running several evaluations with constant parameters as is required for reliable period estimation, and to ensure stable walking over a wide region of parameter space. In addition, we adjusted the center of mass parameter θ_C that is added to the leg standing angle during the evaluation, in order to select for flexibility of movement direction. Measurements of forward and perpendicular distance covered (y_j and x_j respectively) were made over three stages ($j = 1$ to $j = 3$) of length 10 seconds each, as shown in Figure 2A.

We used four fitness functions to simultaneously select for desired capabilities of the robot. The first three correspond to the targeted behaviours for each stage of the evaluation (fast backward motion, steady forward motion and fast forward motion, respectively), while the fourth selects for overall stability. The fitnesses are given as:

$$F_1 = -y_1 - \left(\frac{x_1}{x_0}\right)^2 \quad (9)$$

$$F_2 = 2y_0y_2 - y_2^2 - \left(\frac{x_1}{x_0}\right)^2 \quad (10)$$

$$F_3 = y_3 - \left(\frac{x_1}{x_0}\right)^2 \quad (11)$$

$$F_4 = \frac{y_0^2 H_{\text{tot}}}{1 + t_{\text{tot}}} \quad (12)$$

where $x_0 = \sqrt{5}$ m is a parameter to punish sideways movement, $y_0 = 2.5$ m is an optimal forward distance for steady motion, defining the maximum F_2 and F_4 , H_{tot} is the mean height over the entire evaluation (normalized for a maximum of ≈ 1), and t_{tot} is the root mean square body tilt (mean length of the cross product $\hat{\mathbf{n}} \times \hat{\mathbf{g}}$ where $\hat{\mathbf{n}}$ is the unit vector normal to the top of the robot and $\hat{\mathbf{g}}$ is the unit vector normal to the ground).

Note that F_1 and F_3 are unbounded and identical but with opposite signs for the forward distance. F_2 , meanwhile, is a quadratic function that is positive only between $y_2 = 0$ and $y_2 = 2y_0$. To optimize all four fitness functions simultaneously, the robot must first walk backwards with a negative center of mass parameter, then walk forwards 2.5 m with a positive center of mass parameter and brain stem input of $I_{DC} = 0.5$, and then accelerate with I_{DC} increasing.

During the evolution, the evaluation was run three times per individual with random initial u_i values, and the median of each fitness was taken. For each morphology, five independent populations of 168 individuals (8 individuals per edge of the reference Pareto front) were evolved for 200 generations. The final populations were then evaluated 15 times with different random number generator seeds and the median fitnesses were calculated again, as well as cross-correlations between limbs, and oscillation periods from the largest autocorrelation peak (see Supplementary Material).

2.5 Filter evolution

In order to reduce the total number of evolutions for the filter layer, a subset of CPGs was chosen from each population’s Pareto front in order to capture a numerically small but diverse range of solutions. Each population was first reduced to a set of CPGs for which all fitnesses were positive, and then four were chosen from each using the maxima of four weighted fitness functions F_m^* . These are defined as a combination of F_m and the total sum of fitnesses:

$$F_m^* = zF_m + \sum_{k=1}^4 F_k, \quad (13)$$

where z was incremented in intervals of one until the maximum of each F_m^* was unique.

For each of these CPGs, a 6-neuron, a filter module was evolved using the NSGA3 algorithm. The parameters consisted of 6 input weights, 24 output weights, 30 inhibitory connection weights within the layer, a shared bias term c_i , and the time constant of a low-pass filter for the initial input.

The filter evolution comprised two stages of increasing complexity. The input consisted of evenly spaced impulses with every fourth impulse missing, over a total of 40 seconds. For the first 50 generations, the timings had no noise, in order to facilitate the random generation of suitable filters. After the 50th generation, a random timing offset (Gaussian distributed with a standard deviation of 2% of the period) was applied to each impulse’s timing. Evaluations were made with constant control parameters $\theta_C = 0$ and $I_{DC} = 0.5$.

Three input periods were used for each evaluation: T_0/ϕ , T_0 and ϕT_0 , where T_0 is the CPG period at $\theta_C = 0$ and $I_{DC} = 0.5$, and $\phi = 0.618$. The latter was chosen so that

$1/\phi \approx 1 + \phi$ and hence the low-period and high-period inputs are equidistant from an integer multiple of T_0 .

The fitness function for each input period $T_{in,k}$, with measured walking period $T_{out,k}$, was calculated as

$$F_{fk} = H_{tot,k} Q_k \quad (14)$$

where

$$Q_k = \left(1 + \frac{1}{\epsilon} \left| \frac{2T_{out,k}}{T_{in,k}} - \left[\frac{2T_{out,k}}{T_{in,k}} \right] + \frac{\sigma_0}{\sigma_t} \right| \right)^{-1}, \quad (15)$$

[.] indicates rounding to the nearest integer, σ_0 is the mean standard deviation of the filter output with no input, and σ_t and ϵ are scaling thresholds, both set to 0.1 for the current study. Hence, the fitness is maximized for upright walking with a period of a half-integer or integer multiple of the input period.

The filter evolution used a population of 92 individuals (12 individuals per edge of the reference Pareto front) for 150 generations. At the final generation, the population was evaluated 5 times and the median fitnesses were calculated. This final evaluation included two additional periods at $T_0/\sqrt{\phi}$ and $\sqrt{\phi}T_0$. The filter with the highest $\sum_k Q_k$ was then chosen for each CPG, conditional on each $H_{tot,k}$ being above 0.75.

3 Results

3.1 CPG evolution

From the CPG evolution, 710 unique individuals were produced. As shown in Figure 2B, the fitnesses with upper limits (F_2 and F_4) reached these within a few generations, while the others reached a plateau close to the 200 generation mark.

3.2 Gait characteristics

After filtering out CPGs with an average height of < 0.75 (below which robots were typically judged to be crawling rather than walking, see Supplementary Figure S1), CPGs were classified into gait types. Walking gaits were defined as those with maximum inter-limb correlation < 0.3 ; above this threshold, trotting gaits were defined as those with diagonally opposite limbs maximally correlated, pacing gaits had left or right leg pairs maximally correlated, and bounding gaits were defined as those with front or back limbs maximally correlated. Of the 420 non-crawling individuals at $I_{DC} = 0.5$, $\theta_C = 0.016$, 19.8% were classed as walking, 73.8% as trotting, 2.4% as pacing and 4.0% as bounding. The longer legged robot was more likely to develop a walking gait (29% vs 6%) or bound gait (7% vs 0%), while the short-legged variant was more likely to develop a pacing gait (6% vs 0%).

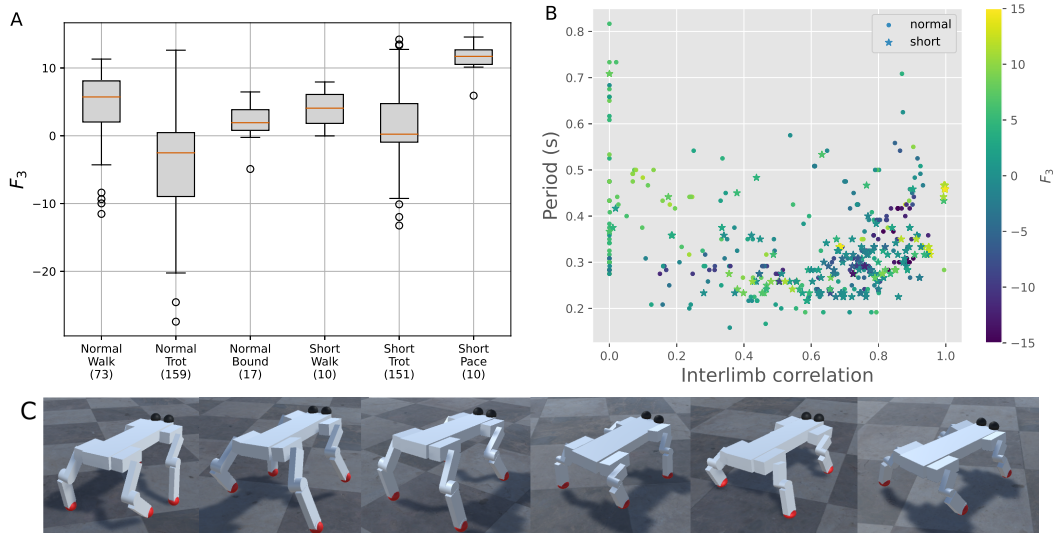


Figure 3: F_3 as a function of morphology and CPG properties, for all upright robots. The box plot (A) shows the distributions of F_3 sorted by morphology and gait types. Numbers in parentheses indicate the number of each gait type in the population. In panel (B) F_3 is plotted as a marker colour against the oscillation period and maximum interlimb correlation of each CPG. For both plots, CPGs are evaluated at $I_{DC} = 0.5, \theta_C = 0.016$. Panel (C) shows images from the simulation for example individuals displaying each of the gaits and body combinations in panel A.

3.3 Predictors of F_3

Many CPGs (14%) were able to have all-positive fitnesses, which means that they could walk backwards and then forwards at a controlled speed as the leg standing angle θ_C is switched from negative to positive. Of particular interest for entrainment is F_3 , the target for acceleration with increasing I_{DC} . This was found to be significantly larger on average in walking and pacing gaits compared to trotting and bounding, contrary to the typical order of quadruped gaits (see Figure 3A).

We examined whether F_3 selected for period or gait flexibility as predicted. For both morphologies, period and F_3 had a non-monotonic relationship with interlimb correlation at $I_{DC} = 0.5$, as shown by Figure 3B. A clear correlation was seen, however, between F_3 and the change in a CPG’s inter-limb correlation as the brain-stem drive was changed from $I_{DC} = 0.5$ to $I_{DC} = 1.0$. This was shown by a linear mixed-effect model with sums and differences of the periods and inter-limb correlations as fixed effects, and replicate as a random effect (long-legged: $z = -2.17, P = 0.03$; short-legged: $z = -3.26, P = 0.001$, see Supplementary Figure S3). This indicates that acceleration leading to a high F_3 could be achieved by moving from a correlated trotting gait towards a more efficient walk-like gait. In addition, for the shorter legged morphology, a period that shortens with increasing I_{DC} is associated with higher F_3 score ($z = -2.72, P = 0.007$, see Supplementary Material).

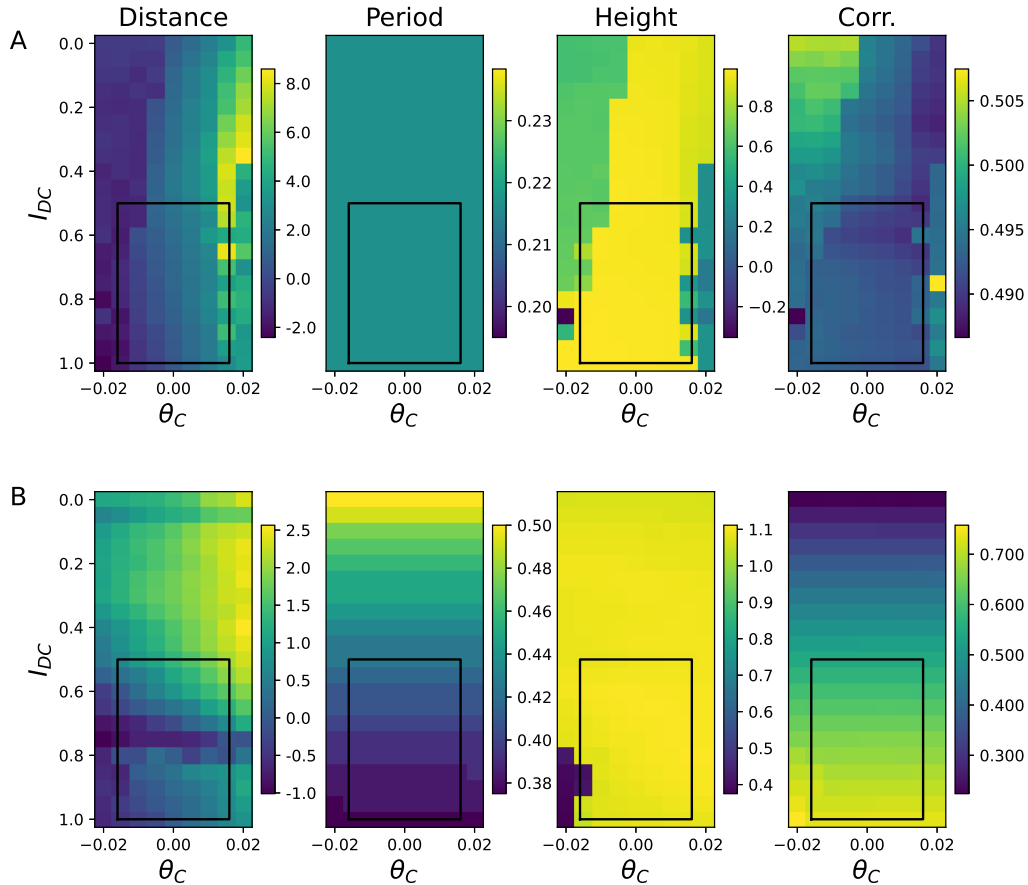


Figure 4: Properties of the CPG with (A) the highest average fitness and (B) the highest negative change in period with I_{DC} as a function of the two control parameters when both are held constant. The black line indicates the range of parameters swept during the evolution. Corr.: Maximum inter-limb correlation coefficient.

3.4 Direction and speed tuning

The trained robots typically show regions of smooth change of speed and direction within the space of control parameters. These regions often extend outside the region of the control parameter sweeps. Two examples are shown in Figure 4. For the CPG that maximized the average CPG evolution fitnesses (Eqs 9-12), the brain stem drive I_{DC} has relatively little effect on the movement characteristics. This illustrates that high average fitness is itself not a guarantee of general flexibility. Further outside the region of the swept control parameters, the behaviour becomes more unpredictable. For example, the low measured height in Figure 4A for low drive parameter and negative θ_C indicates an instability that coincides with a gait transition, as shown by an abrupt change in inter-limb correlation in the same region.

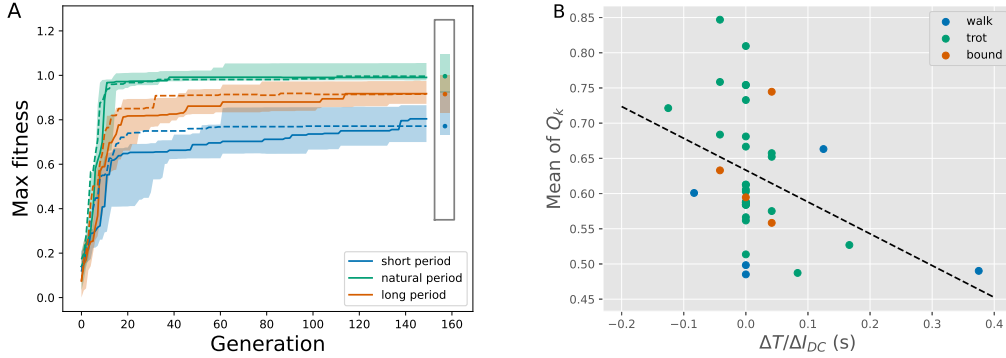


Figure 5: Filter evolution. Panel (A) shows the maximum fitnesses F_{fk} vs generation for the three input periods. Solid lines: normal quadruped; dotted lines: short-legged variant. Each line is the median over 19 CPGs used as the basis. Shaded areas are the interquartile range over the 19 CPGs for the normal quadruped. Areas inside the box on the right side of the plot are the final interquartile ranges of maximum fitness for the short-legged variant. Panel (B) shows the total entrainment ability score $\sum_{k=1}^3 Q_k/3$ for all robots over the height threshold for each k , as a function of period flexibility (gradient in period vs brain stem drive, with $\Delta I_{DC} = 0.2$). The dotted line is the best fit from the linear regression.

3.5 Filter evolution

Each morphology had 19 CPGs chosen for filter evolution out of the planned 20. One long-legged replicate only produced three unique CPGs from Equation 13, while one selected CPG from the short-legged replicates had no measurable walking period, so an input period could not be determined.

The evolution of the filter module is shown in Figure 5A. The short-legged morphology converged to the maximum fitness sooner than the long-legged morphology. In general, it was more difficult to entrain to a rhythmic input shorter than the natural walking period, compared to a longer period input.

3.6 Predictors of entrainment

When taking the highest eligible mean of the entrainment performance Q_k , a correlation was found between the period tunability and entrainment performance (linear model: $t = -2.26$, $P = 0.03$, see Figure 5B). Faster oscillation with increasing I_{DC} therefore facilitates entrainment, while faster oscillation with decreasing I_{DC} appears to inhibit this ability. For the highest fitness filter and CPG combinations, entrainment could be generalized to stimulus periods other than those used during evolution, as shown in Figure 6. Adjustment to the stimulus turning on or off typically occurred within a few motion cycles. To show this, time series for the leg joint angles were convolved with a Morlet wavelet at the input period, with a resolution parameter $\sigma = 1.5$, and then a Gaussian filter was applied with a width of 0.5 s.

Interestingly, the robot could generate a response that created a polyrhythm with the input (namely, two steps for every three impulses), as shown in Figure 6A.

4 Discussion

Our highly nonlinear, bio-inspired central pattern generator combined with multi-objective optimization was successful in both generating a variety of gait profiles and properties, as well as flexibility in these gaits for a large subset of individuals. This was despite the fact that the fitness functions did not straightforwardly translate to specific gait properties.

Trots were the most favoured gait type for both morphologies, seemingly due to this gait’s ability to transition from backwards to forwards motion. The short-legged robot was more predictable, as evidenced by its smaller range of fitnesses for each gait type, and evolved faster in the case of the filter layer. Hence, it can be used as a starting point for building complex behaviour in stages [58].

Notably, the gait frequency emerged in a self-organized fashion from the interactions in the CPG network and — due to the added nonlinearities of the neural model — was also sensitive to inputs. Oscillation periods could therefore be tuned both manually via the brainstem drive parameter, and automatically via spontaneous entrainment to fluctuating sensory input. Due to the fully self-organized nature of the entrainment, this occurred much more rapidly than feedback-based approaches [5, 59, 42]. We expect similar results if utilizing other neuron models with input-dependent frequency, such as the Fitzhugh-Nagumo model [60] or the Rowat-Selverston model [36]. Phase synchronization to stimulus may be achieved in the future by adding feedback from reaction forces, such as with the *Tegotae* approach [61].

The specific results in this article can also be used to further direct the evolution of desired behaviours. For example, entrainment appears to benefit from a period that decreases with input, as occurs in single biological neurons. Restricting parameters to ensure this can increase the speed of evolution and the likelihood of entrainment. While the fitness targeting fast forward movement was significantly correlated with period flexibility, the period ranges exhibited were not as wide as when directly using the latter explicitly as a fitness function, as was done in [46]. Therefore, a combined approach where a disembodied CPG is first evolved may be beneficial in future work.

Rhythmic entrainment is a complex behaviour seen only in very few species [62], and is thought to be an integral part of the evolution of human social behaviour. Our CPG network mediated by a filter layer successfully captures this important example of cortical shaping of cyclical movements. Our heavily bio-inspired approach offers a path towards testing theories of human cognitive processes, such as beat perception, that are still not well understood [63, 64]. The results we present show that dynamic attending theory, based on synchronization of endogenous rhythms [65, 66], is a viable explanation for beat perception also when involving an entire distributed sensorimotor system.

On the engineering side, this approach is highly relevant to the current push towards adaptive robot behaviour [2, 11, 23]. In this study, the filter layer was optimized by a genetic

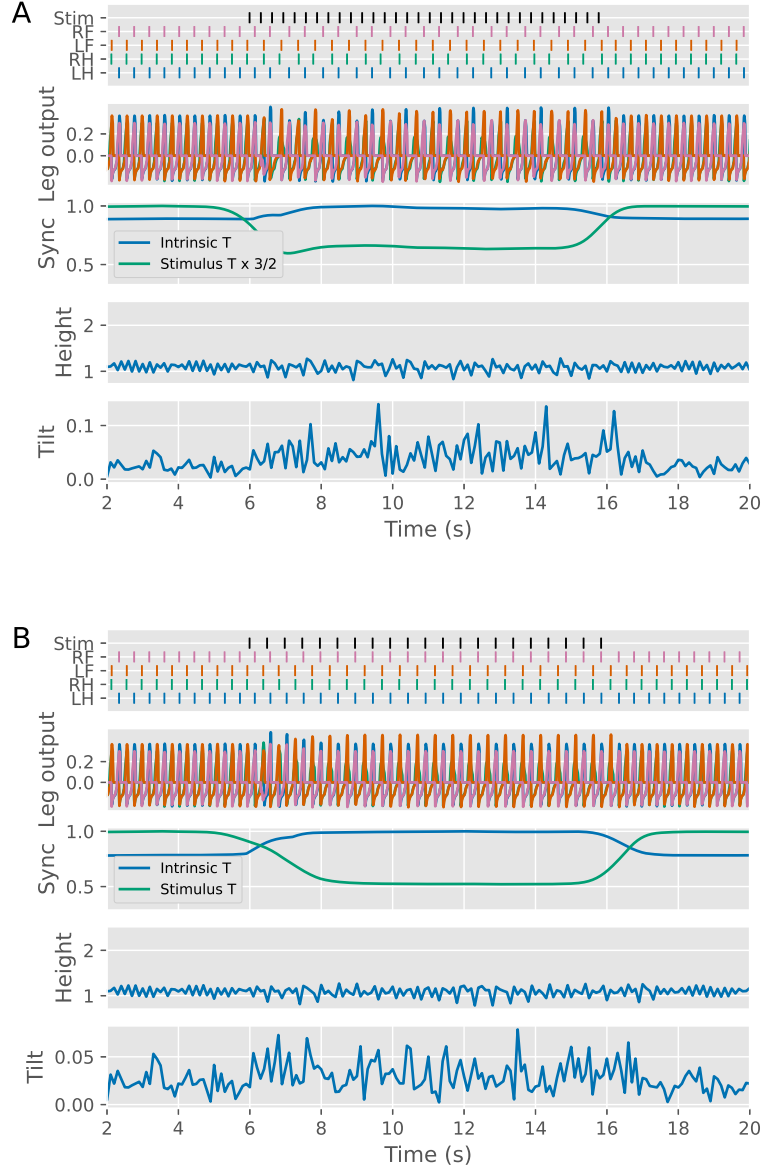


Figure 6: Entrainment to an isochronous stimulus at **(A)** 80% and **(B)** 125% of the natural period, respectively, for the CPG with highest negative change in period with I_{DC} . The stimulus is started at the 8 second mark, and ends at the 16 second mark. Black ticks show the impulse times for the stimulus, and the peaks of the leg output below, corresponding to the extent of the forward swings in radians. Sync: output from the smoothed Morlet wavelet convolution, normalized to a maximum of one.

algorithm. However, by instead adding Hebbian plasticity [67], reinforcement learning [34] or another mechanism for longer-term adaptation, it may be possible for robots to learn suitable new movement patterns through repeated imitation of robot or human demonstrators in an unsupervised manner, and hence develop useful behaviours autonomously [68].

Future work will implement physical robots with performance metrics addressing movement efficiency and stability in different physical environments. We will also explore mutual adaptation of multiple robots by using foot sensors to transmit impulses to neighbours. Notably, the fact that the communication medium is a simple time series means that coordination can occur across differing morphologies. This is also likely to increase the complexity of the behaviours, as is typical in studies of collective motion [69], and may allow for creative uses, such as human-robot musical ensembles [70].

Acknowledgments

This project has received funding from the European Union’s Horizon 2020 research and innovation programme under the Marie Skłodowska-Curie grant agreement No 101030688, and is partially supported by the Research Council of Norway through its Centres of Excellence scheme, project number 262762. The authors would also like to thank Caroline Palmer and Anne Danielsen for helpful discussions.

Data Availability Statement

The code used and datasets generated for this study can be found at the project Github: <https://github.com/aszorko/COROBOREES/tree/Paper2>

References

References

- [1] A. J. Ijspeert, “Central pattern generators for locomotion control in animals and robots: a review,” *Neural networks*, vol. 21, no. 4, pp. 642–653, 2008.
- [2] S. Aoi, P. Manoonpong, Y. Ambe, F. Matsuno, and F. Wörgötter, “Adaptive control strategies for interlimb coordination in legged robots: a review,” *Frontiers in neuro-robotics*, vol. 11, p. 39, 2017.
- [3] S. Dasgupta, D. Goldschmidt, F. Wörgötter, and P. Manoonpong, “Distributed recurrent neural forward models with synaptic adaptation and cpg-based control for complex behaviors of walking robots,” *Frontiers in neurorobotics*, vol. 9, p. 10, 2015.

- [4] S. Steingrube, M. Timme, F. Wörgötter, and P. Manoonpong, “Self-organized adaptation of a simple neural circuit enables complex robot behaviour,” *Nature physics*, vol. 6, no. 3, pp. 224–230, 2010.
- [5] J. Buchli, F. Iida, and A. J. Ijspeert, “Finding resonance: Adaptive frequency oscillators for dynamic legged locomotion,” in *2006 IEEE/RSJ International Conference on Intelligent Robots and Systems*. IEEE, 2006, pp. 3903–3909.
- [6] T. Iwasaki and M. Zheng, “Sensory feedback mechanism underlying entrainment of central pattern generator to mechanical resonance,” *Biological cybernetics*, vol. 94, no. 4, pp. 245–261, 2006.
- [7] K. Seo, S.-J. Chung, and J.-J. E. Slotine, “Cpg-based control of a turtle-like underwater vehicle,” *Autonomous Robots*, vol. 28, no. 3, pp. 247–269, 2010.
- [8] R. Thandiackal, K. Melo, L. Paez, J. Herault, T. Kano, K. Akiyama, F. Boyer, D. Ryczko, A. Ishiguro, and A. J. Ijspeert, “Emergence of robust self-organized undulatory swimming based on local hydrodynamic force sensing,” *Science Robotics*, vol. 6, no. 57, p. eabf6354, 2021.
- [9] C. Maufroy, H. Kimura, and K. Takase, “Integration of posture and rhythmic motion controls in quadrupedal dynamic walking using phase modulations based on leg loading/unloading,” *Autonomous Robots*, vol. 28, no. 3, pp. 331–353, 2010.
- [10] Y. Fukuoka, Y. Habu, and T. Fukui, “A simple rule for quadrupedal gait generation determined by leg loading feedback: a modeling study,” *Scientific reports*, vol. 5, no. 1, pp. 1–11, 2015.
- [11] O. Nocentini, L. Fiorini, G. Acerbi, A. Sorrentino, G. Mancioffi, and F. Cavallo, “A survey of behavioral models for social robots,” *Robotics*, vol. 8, no. 3, p. 54, 2019.
- [12] G. Knoblich and N. Sebanz, “Evolving intentions for social interaction: from entrainment to joint action,” *Philosophical Transactions of the Royal Society B: Biological Sciences*, vol. 363, no. 1499, pp. 2021–2031, 2008.
- [13] G. Tomlinson, *A million years of music: The emergence of human modernity*. Zone Books, 2015.
- [14] S. Kotz, A. Ravignani, and W. Fitch, “The evolution of rhythm processing,” *Trends in Cognitive Sciences*, vol. 22, no. 10, pp. 896–910, 2018.
- [15] S. M. Danner, N. A. Shevtsova, A. Frigon, and I. A. Rybak, “Computational modeling of spinal circuits controlling limb coordination and gaits in quadrupeds,” *Elife*, vol. 6, p. e31050, 2017.

- [16] R. D. Beer, R. D. Quinn, H. J. Chiel, and R. E. Ritzmann, “Biologically inspired approaches to robotics: What can we learn from insects?” *Communications of the ACM*, vol. 40, no. 3, pp. 30–38, 1997.
- [17] A. J. Ijspeert, “A connectionist central pattern generator for the aquatic and terrestrial gaits of a simulated salamander,” *Biological cybernetics*, vol. 84, no. 5, pp. 331–348, 2001.
- [18] T. Sun, X. Xiong, Z. Dai, D. Owaki, and P. Manoonpong, “A comparative study of adaptive interlimb coordination mechanisms for self-organized robot locomotion,” *Frontiers in Robotics and AI*, vol. 8, p. 638684, 2021.
- [19] M. Chen, X. Mo, Y. Zhang, and S. Wang, “Research on fusion control of sensor information and biological reflection based on cpg,” *Advances in Mechanical Engineering*, vol. 15, no. 1, p. 16878132221149560, 2023.
- [20] C. Liu, Q. Chen, and D. Wang, “Cpg-inspired workspace trajectory generation and adaptive locomotion control for quadruped robots,” *IEEE Transactions on Systems, Man, and Cybernetics, Part B (Cybernetics)*, vol. 41, no. 3, pp. 867–880, 2011.
- [21] Y. Nakamura, T. Mori, M.-a. Sato, and S. Ishii, “Reinforcement learning for a biped robot based on a cpg-actor-critic method,” *Neural networks*, vol. 20, no. 6, pp. 723–735, 2007.
- [22] M. Thor, B. Strohmer, and P. Manoonpong, “Locomotion control with frequency and motor pattern adaptations,” *Frontiers in Neural Circuits*, vol. 15, 2021.
- [23] H. Ravichandar, A. Polydoros, S. Chernova, and A. Billard, “Recent advances in robot learning from demonstration,” *Annual Review of Control, Robotics, and Autonomous Systems*, vol. 3, pp. 297–330, 2020.
- [24] J. C. Bongard, “Evolutionary robotics,” *Communications of the ACM*, vol. 56, no. 8, pp. 74–83, 2013.
- [25] S. Doncieux, N. Bredeche, J.-B. Mouret, and A. E. Eiben, “Evolutionary robotics: what, why, and where to,” *Frontiers in Robotics and AI*, vol. 2, p. 4, 2015.
- [26] K. Deb and H. Jain, “An evolutionary many-objective optimization algorithm using reference-point-based nondominated sorting approach, part i: solving problems with box constraints,” *IEEE transactions on evolutionary computation*, vol. 18, no. 4, pp. 577–601, 2013.
- [27] J. B. Mouret, “Evolving the Behavior of Machines: From Micro to Macroevolution,” *iScience*, vol. 23, no. 11, p. 101731, 2020. [Online]. Available: <https://doi.org/10.1016/j.isci.2020.101731>

- [28] J. Collins, D. Howard, W. Geles, and F. Maire, “Towards the targeted environment-specific evolution of robot components,” *GECCO 2018 - Proceedings of the 2018 Genetic and Evolutionary Computation Conference*, pp. 61–68, 2018.
- [29] N. Cheney, R. MacCurdy, J. Clune, and H. Lipson, “Unshackling Evolution: Evolving Soft Robots with Multiple Materials and a Powerful Generative Encoding,” *Proceeding of the Fifteenth Annual Conference on Genetic and Evolutionary Computation - GECCO '13*, p. 167, 2013.
- [30] J. Nordmoen, F. Veenstra, K. O. Ellefsen, and K. Glette, “Map-elites enables powerful stepping stones and diversity for modular robotics,” *Frontiers in Robotics and AI*, vol. 8, p. 639173, 2021.
- [31] F. Veenstra and K. Glette, “How different encodings affect performance and diversification when evolving the morphology and control of 2d virtual creatures,” in *Artificial Life Conference Proceedings*. MIT Press, 2020, pp. 592–601.
- [32] K.-i. Funahashi and Y. Nakamura, “Approximation of dynamical systems by continuous time recurrent neural networks,” *Neural networks*, vol. 6, no. 6, pp. 801–806, 1993.
- [33] D. Floreano, P. Dürri, and C. Mattiussi, “Neuroevolution: from architectures to learning,” *Evolutionary intelligence*, vol. 1, no. 1, pp. 47–62, 2008.
- [34] J. Hwangbo, J. Lee, A. Dosovitskiy, D. Bellicoso, V. Tsounis, V. Koltun, and M. Hutter, “Learning agile and dynamic motor skills for legged robots,” *Science Robotics*, vol. 4, no. 26, p. eaau5872, 2019.
- [35] P. Arena, S. De Fiore, L. Patané, M. Pollino, and C. Ventura, “Stdp-based behavior learning on the tribot robot,” in *Bioengineered and Bioinspired Systems IV*, vol. 7365. SPIE, 2009, pp. 49–59.
- [36] M. Jouaiti, L. Caron, and P. Hénaff, “Hebbian plasticity in cpg controllers facilitates self-synchronization for human-robot handshaking,” *Frontiers in neurorobotics*, vol. 12, p. 29, 2018.
- [37] T. Reil and P. Husbands, “Evolution of central pattern generators for bipedal walking in a real-time physics environment,” *IEEE Transactions on evolutionary computation*, vol. 6, no. 2, pp. 159–168, 2002.
- [38] M. Oliveira, C. P. Santos, L. Costa, V. Matos, and M. Ferreira, “Multi-objective parameter cpg optimization for gait generation of a quadruped robot considering behavioral diversity,” in *2011 IEEE/RSJ International Conference on Intelligent Robots and Systems*. IEEE, 2011, pp. 2286–2291.
- [39] C. Liu, H. Xiao, D. Wang, and Q. Chen, “Evolution of neural oscillator network for the biped walking control of a four-link robot,” in *2015 IEEE International Conference on Information and Automation*. IEEE, 2015, pp. 2305–2310.

- [40] B. Wang, X. Cui, J. Sun, and Y. Gao, “Parameters optimization of central pattern generators for hexapod robot based on multi-objective genetic algorithm,” *International Journal of Advanced Robotic Systems*, vol. 18, no. 5, p. 17298814211044934, 2021.
- [41] C. Chambers, G. Kong, K. Wei, and K. Kording, “Pose estimates from online videos show that side-by-side walkers synchronize movement under naturalistic conditions,” *PloS one*, vol. 14, no. 6, p. e0217861, 2019.
- [42] Y. Miyake, “Interpersonal synchronization of body motion and the walk-mate walking support robot,” *IEEE Transactions on Robotics*, vol. 25, no. 3, pp. 638–644, 2009.
- [43] N. Rudin, H. Kolvenbach, V. Tsounis, and M. Hutter, “Cat-like jumping and landing of legged robots in low gravity using deep reinforcement learning,” *IEEE Transactions on Robotics*, vol. 38, no. 1, pp. 317–328, 2021.
- [44] E. Medvet, G. Nadizar, and F. Pigozzi, “On the impact of body material properties on neuroevolution for embodied agents: the case of voxel-based soft robots,” in *Proceedings of the Genetic and Evolutionary Computation Conference Companion*, 2022, pp. 2122–2130.
- [45] J.-B. Mouret and J. Clune, “Illuminating search spaces by mapping elites,” *arXiv preprint arXiv:1504.04909*, 2015.
- [46] A. Szorkovszky, F. Veenstra, and K. Glette, “Rapid rhythmic entrainment in bio-inspired central pattern generators,” in *2022 International Joint Conference on Neural Networks (IJCNN)*. IEEE, 2022.
- [47] T. F. Nygaard, C. P. Martin, J. Torresen, K. Glette, and D. Howard, “Real-world embodied ai through a morphologically adaptive quadruped robot,” *Nature Machine Intelligence*, vol. 3, no. 5, pp. 410–419, 2021.
- [48] K. Matsuoka, “Sustained oscillations generated by mutually inhibiting neurons with adaptation,” *Biological cybernetics*, vol. 52, no. 6, pp. 367–376, 1985.
- [49] G. Taga, Y. Yamaguchi, and H. Shimizu, “Self-organized control of bipedal locomotion by neural oscillators in unpredictable environment,” *Biological cybernetics*, vol. 65, no. 3, pp. 147–159, 1991.
- [50] H. Kimura, S. Akiyama, and K. Sakurama, “Realization of dynamic walking and running of the quadruped using neural oscillator,” *Autonomous robots*, vol. 7, no. 3, pp. 247–258, 1999.
- [51] T. Fukui, H. Fujisawa, K. Otaka, and Y. Fukuoka, “Autonomous gait transition and galloping over unperceived obstacles of a quadruped robot with cpg modulated by vestibular feedback,” *Robotics and Autonomous Systems*, vol. 111, pp. 1–19, 2019.

- [52] M. Jouaiti and P. Henaff, “Comparative study of forced oscillators for the adaptive generation of rhythmic movements in robot controllers,” *Biological cybernetics*, vol. 113, no. 5, pp. 547–560, 2019.
- [53] K. Matsuoka, “Mechanisms of frequency and pattern control in the neural rhythm generators,” *Biological cybernetics*, vol. 56, no. 5, pp. 345–353, 1987.
- [54] F. K. Skinner, N. Kopell, and E. Marder, “Mechanisms for oscillation and frequency control in reciprocally inhibitory model neural networks,” *Journal of computational neuroscience*, vol. 1, no. 1, pp. 69–87, 1994.
- [55] F. Grimmering, A. Meduri, M. Khadiv, J. Viereck, M. Wüthrich, M. Naveau, V. Berenz, S. Heim, F. Widmaier, T. Flayols, J. Fiene, A. Badri-Spröwitz, and L. Righetti, “An open torque-controlled modular robot architecture for legged locomotion research,” *IEEE Robotics and Automation Letters*, vol. 5, no. 2, pp. 3650–3657, 2020.
- [56] A. Juliani, V.-P. Berges, E. Teng, A. Cohen, J. Harper, C. Elion, C. Goy, Y. Gao, H. Henry, M. Mattar *et al.*, “Unity: A general platform for intelligent agents,” *arXiv preprint arXiv:1809.02627*, 2018.
- [57] F.-A. Fortin, F.-M. De Rainville, M.-A. Gardner, M. Parizeau, and C. Gagné, “DEAP: Evolutionary algorithms made easy,” *Journal of Machine Learning Research*, vol. 13, pp. 2171–2175, jul 2012.
- [58] J. Bongard, “Morphological change in machines accelerates the evolution of robust behavior,” *Proceedings of the National Academy of Sciences*, vol. 108, no. 4, pp. 1234–1239, 2011.
- [59] G. Brambilla, J. Buchli, and A. J. Ijspeert, “Adaptive four legged locomotion control based on nonlinear dynamical systems,” in *From Animals to Animats 9: 9th International Conference on Simulation of Adaptive Behavior, SAB 2006, Rome, Italy, September 25-29, 2006. Proceedings 9*. Springer, 2006, pp. 138–149.
- [60] J. Nagumo, S. Arimoto, and S. Yoshizawa, “An active pulse transmission line simulating nerve axon,” *Proceedings of the IRE*, vol. 50, no. 10, pp. 2061–2070, 1962.
- [61] D. Owaki, M. Goda, S. Miyazawa, and A. Ishiguro, “A minimal model describing hexapedal interlimb coordination: the tegotae-based approach,” *Frontiers in neuro-robotics*, vol. 11, p. 29, 2017.
- [62] F. L. Bouwer, V. Nityananda, A. A. Rouse, and C. Ten Cate, “Rhythmic abilities in humans and non-human animals: A review and recommendations from a methodological perspective,” *Philosophical Transactions of the Royal Society B*, vol. 376, no. 1835, p. 20200335, 2021.
- [63] S. Koelsch, P. Vuust, and K. Friston, “Predictive processes and the peculiar case of music,” *Trends in cognitive sciences*, vol. 23, no. 1, pp. 63–77, 2019.

- [64] P. Lakatos, J. Gross, and G. Thut, “A new unifying account of the roles of neuronal entrainment,” *Current Biology*, vol. 29, no. 18, pp. R890–R905, 2019.
- [65] E. W. Large and M. R. Jones, “The dynamics of attending: How people track time-varying events.” *Psychological review*, vol. 106, no. 1, p. 119, 1999.
- [66] C. Palmer and A. P. Demos, “Are we in time? how predictive coding and dynamical systems explain musical synchrony,” *Current Directions in Psychological Science*, vol. 31, no. 2, pp. 147–153, 2022.
- [67] R. Kempter, W. Gerstner, and J. L. Van Hemmen, “Hebbian learning and spiking neurons,” *Physical Review E*, vol. 59, no. 4, p. 4498, 1999.
- [68] A. F. Winfield and M. D. Erbas, “On embodied memetic evolution and the emergence of behavioural traditions in robots,” *Memetic Computing*, vol. 3, pp. 261–270, 2011.
- [69] D. J. Sumpter, *Collective animal behavior*. Princeton University Press, 2010.
- [70] M. Krzyżaniak, “Musical robot swarms, timing, and equilibria,” *Journal of New Music Research*, vol. 50, no. 3, pp. 279–297, 2021.

Supplementary Material

Parameter ranges

Table S1 shows both fixed parameters (single numbers) and evolvable ranges (inside square brackets) for the CPG module. Connection weights w_{ij} are zero between limbs, apart from when i and j are both interneurons (see main text Figure 1A).

Parameter ranges for the filter module are shown similarly in Table S2. Here, Γ is the time constant of an exponential low-pass filter for the impulse stimulus.

Finally, parameter ranges for the joint activation and sensory feedback are given in Table S3. These are evolved in the same genotype as the CPG parameters.

Evolution parameters

NSGA-III parameters are shown in Table S4. Here, p_c is the crossover probability and p_m is the mutation probability per allele.

Period and interlimb correlation

The period was determined using the autocorrelation of a complex-valued time series $z(t) = x(t) + iy(t)$ where $x(t)$ and $y(t)$ are the leg and knee neuron outputs before the sigmoidal transform respectively, and where t begins halfway through the evaluation. The time lag for the maximum correlation was extracted, with a minimum of $t_0 \approx 0.05$ seconds. During the filter evolution, a maximum lag of 2.25 times the natural period was imposed. If no peak was found in this region, the CPG was excluded from further analysis.

The location of the highest cluster of average height was determined to be above 0.75, and these CPGs were judged to be upright for the entire trial (see Figure S1). The cluster of lower average heights corresponds to crawling with knee joints touching the ground, while in between were upright for only part of the trial. All CPGs below 0.75 average height were excluded from further analysis.

The interlimb correlation was determined by the Pearson product-moment correlation over the second half of the evaluation period. Only the leg neuron output was used. A four by four matrix C_{ij} of limbs was set up for the correlation between the i th and j th limb, and only off-diagonal elements were calculated, with diagonal elements C_{ii} being manually set to zero. Therefore if all pairs had negative correlations, the CPG gait was classified as a walk (see Figure S2).

Statistics

Statistical tests were performed using the Python *statsmodels* package. Figure S3 shows the lines of best fit from the linear mixed-effect model for F_3 . Normality of residuals was tested using the Kolmogorov-Smirnov test.

Table S1: Parameter ranges for the CPG network.

Parameter	Value / Range
t_0	0.052 s
γ	[0.01,0.1]
a	[0.2,2]
b	[0.02,0.2]
κ	[0.5,5]
u_0	[0.1,1]
d_i	[-0.9,0.9]
c_i	[1.1,2]
w_{ij}	[-1.8,1.8] / 0

Table S2: Parameter ranges for the filter network

Parameter	Value / Range
t_0	0.052 s
γ	0.03
a	2
b	0.3
κ	4
u_0	1
d_i	0
τ_0	0.15
Γ	[0.05,0.55]
c_i	[2,2.5]
G_i	[-1,1]
w_{ij}	[-1.2,0]
M_{ij}	[-10,10]

Table S3: Parameter ranges for the joint activation and sensory feedback. All angles (θ) are in degrees.

Parameter	Value / Range
$\theta_{0,\text{hip}}$	[2.7, 27]
$\theta_{0,\text{leg}}$	[4.5, 45]
$\theta_{0,\text{knee}}$	-[7.2, -72]
$\theta_{\text{lim,leg}}$	90
$\theta_{\text{lim,knee}}$	90
A	[0.005, 0.05]
B	[0.005, 0.05]
$q_{A,\text{front}}$	[-0.45, 0.45]
$q_{B,\text{front}}$	[-0.45, 0.45]
$q_{A,\text{side}}$	[-0.45, 0.45]
$q_{B,\text{side}}$	[-0.45, 0.45]

Table S4: NSGA-III parameters for each stage of evolution.

	CPG	Filter
N alleles	32	62
N individuals	168	92
N partitions	8	12
N objectives	4	3
N generations	200	150
p_c	0.7	1.0
p_m	0.05	0.05

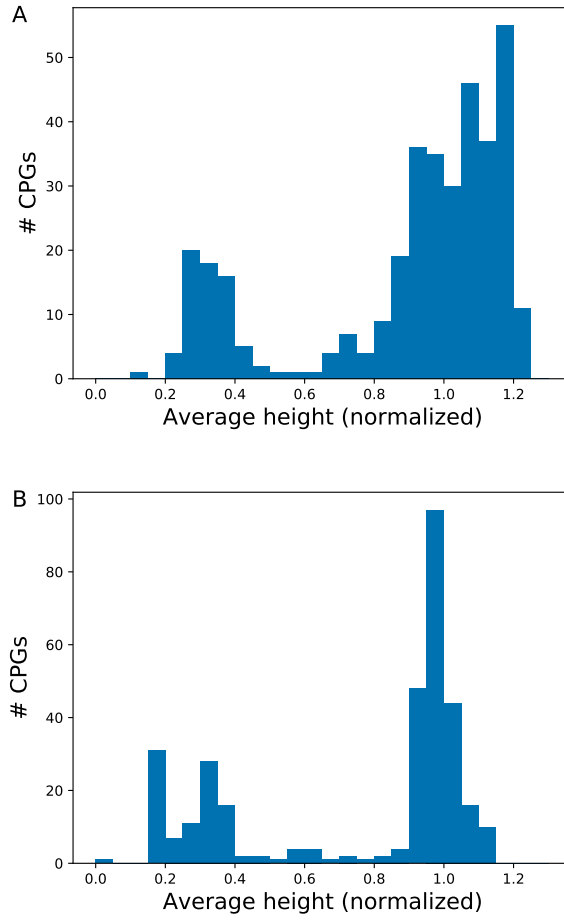


Figure S1: Histograms of average height during one evaluation for (A) all normal quadruped CPGs and (B) all short quadruped CPGs, evaluated at $I_{DC} = 0.5, \theta_C = 0.016$.

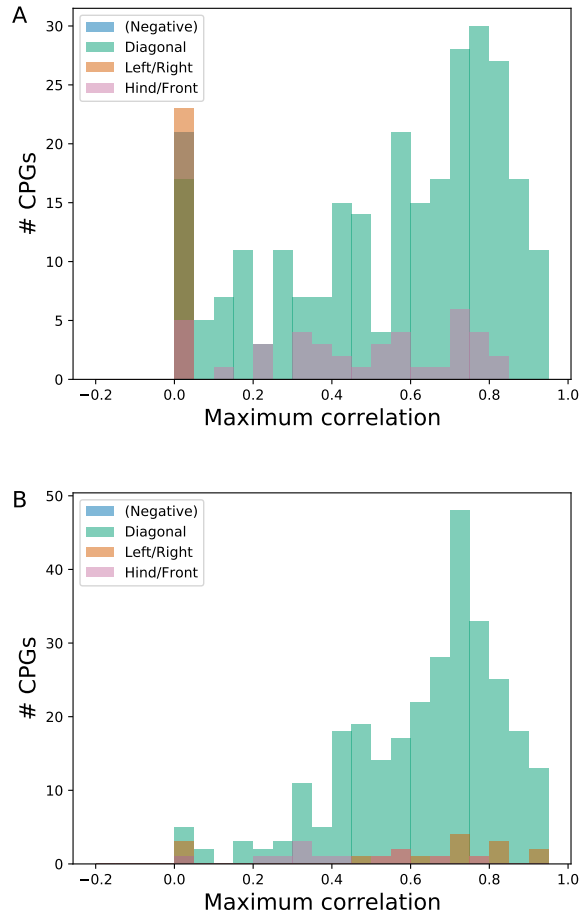


Figure S2: Histograms of maximum correlation, sorted by the most correlated pair of limbs, for (A) all normal quadruped CPGs and (B) all short quadruped CPGs, evaluated at $I_{DC} = 0.5, \theta_C = 0.016$.

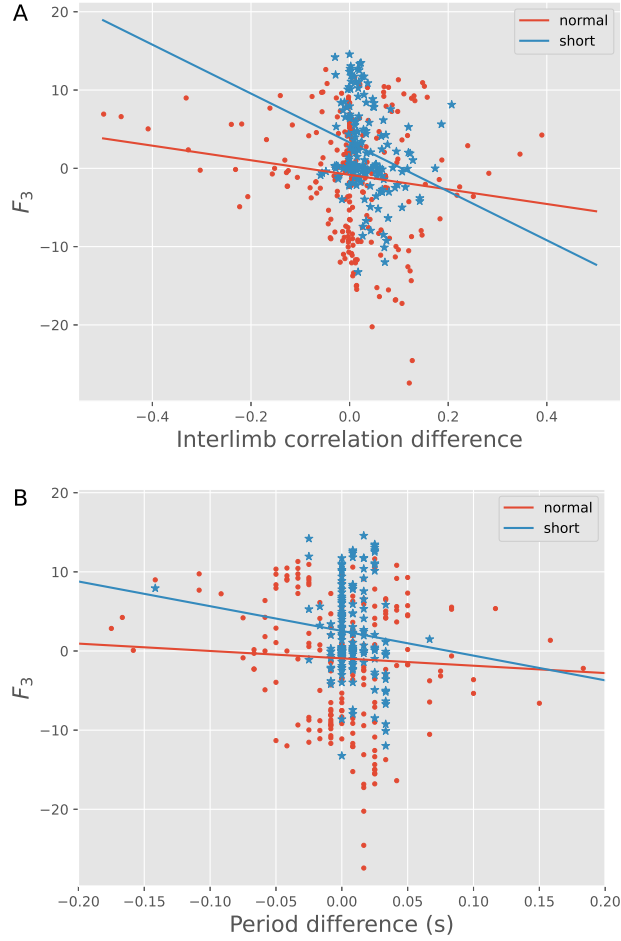


Figure S3: F_3 as a function CPG variability, for all upright robots. Shown are scatter plots of F_3 against **(A)** the change in the maximum inter-limb correlation, and **(B)** the change in period, when increasing I_{DC} from 0.5 to 1. Straight lines indicate the intercept and coefficient of best fit from linear mixed-effect models. In both panels the robots are in forward mode ($\theta_C = 0.016$).